

Angularly resolved observations of sidescattered laser light from laser-produced plasmas

P. E. Young and K. G. Estabrook

University of California, Lawrence Livermore National Laboratory, P.O. Box 5508, Livermore, California 94550

(Received 30 June 1993; revised manuscript received 10 January 1994)

Small scale structure is observed in angularly resolved measurements of scattered laser light from 1.06 μm laser irradiations of CH targets. The structure size varies as the laser spot diameter is changed. The structure is consistent with light produced by the stimulated Brillouin sidescattering instability. The overall angular dependence of the scattered laser light intensity is compared to the distribution predicted by convective growth of stimulated Brillouin sidescattering. Two-dimensional plasma effects are shown to be important in determining the angular distribution of the scattered light.

PACS number(s): 52.35.Fp, 52.35.Nx, 52.40.Nk, 52.50.Jm

I. INTRODUCTION

The understanding of the coupling between lasers and plasmas continues to be a challenging problem. A high intensity laser can excite parametric instabilities in a plasma, one of which is stimulated Brillouin scattering (SBS) [1,2]. The SBS instability is a three-wave interaction of the incident light wave, an ion acoustic wave, and a scattered light wave. The linear theory of SBS growth in an inhomogeneous plasma for light backscattered in the direction of the incident laser has been gradually developed over time [1–9]. Significant growth of SBS sidescattering can occur in large plasmas; the SBS sidescattering gain can be as large as, or larger than, that in the direction of direct backscatter [8,9]. In the past, measurements of sidescattered laser light from laser-produced plasmas have been limited in number and there have been no direct comparisons to theoretical predictions. Although the overall angular dependence of scattered light has been measured with photodiodes [10], this technique does not resolve structure in the scattered light pattern. Angularly resolved measurements using burn paper have been reported [11]; however, this method is sensitive to only the most intense parts of the scattered light distribution, has a limited dynamic range, and requires a high laser intensity to produce detectable signals.

In this paper, we present detailed angularly resolved measurements of sidescattered laser light from 1.06 μm laser interactions with a low Z target material. We have used appropriately filtered film as the recording medium and are able to observe both the angular dependence of the sidescattered laser light and small scale angular structure in the scattered light. Both the angular distribution with respect to the laser polarization and the behavior of the time and spectrum resolved measurements at fixed angles are consistent with light produced by stimulated Brillouin sidescatter. Both analytic theory and simulations, which assume plasmas of infinite transverse extent, predict localized angular spikes of scattered light, which could be missed in experiments using discrete detectors. Our experiments show an angular dependence which can be reproduced by the analytic theory provided that we take into account the two-dimensional extent of the SBS gain region.

In the remainder of this paper, we first describe the experiment and our observations in Sec. II. In Sec. III, we describe our calculations of the predicted angular distribution of scattered light based on convective growth of the stimulated Brillouin scattering instability. The predictions are compared to simulations of ion fluctuations, which might be responsible for the scattered light structure. In Sec. IV we compare the predictions to the observations and discuss the differences. Our conclusions are presented in Sec. V.

II. DESCRIPTION OF THE EXPERIMENT

The experiment used one beam of the Janus laser facility at Lawrence Livermore National Laboratory. The laser was incident normal to the target, had a wavelength equal to 1.06 μm , and was Gaussian in time with a 1 ns full width at half maximum. The beam was focused with an $f/2$, 20 cm focal length lens. We varied the spot size between 100 and 500 μm , while keeping the laser intensity I_L approximately constant by changing the laser energy from 11 to 50 J. The target was a 50 μm thick parylene (carbon-hydrogen) foil which did not burn through during the laser pulse.

The laser pattern at the target plane was obtained by an equivalent plane imaging system with a charge coupled device (CCD) camera as the recording medium. Figure 1 exhibits intensity profiles through the vertical and horizontal planes of the laser spot for spot diameters of 100, 200, and 500 μm . The spot was reasonably symmetric with less than 15% variation in diameter between the two planes. The polarization for most of the measurements described in this paper was oriented vertically.

The scattered light was recorded by Kodak Tri-X film and each exposure was made using a single laser pulse. The recording film was placed at an approximately 60° angle relative to the target plane (see Fig. 2) and either parallel or perpendicular to the plane of polarization on different laser pulses. The film was at all times covered with a 2 mm thick sheet of RG 1000 colored glass, which not only attenuated visible light but also prevented x rays and charged particles from reaching the film. On some exposures, an additional neutral density (with an attenuation factor at 1.06 μm of 10) filter was placed in front of

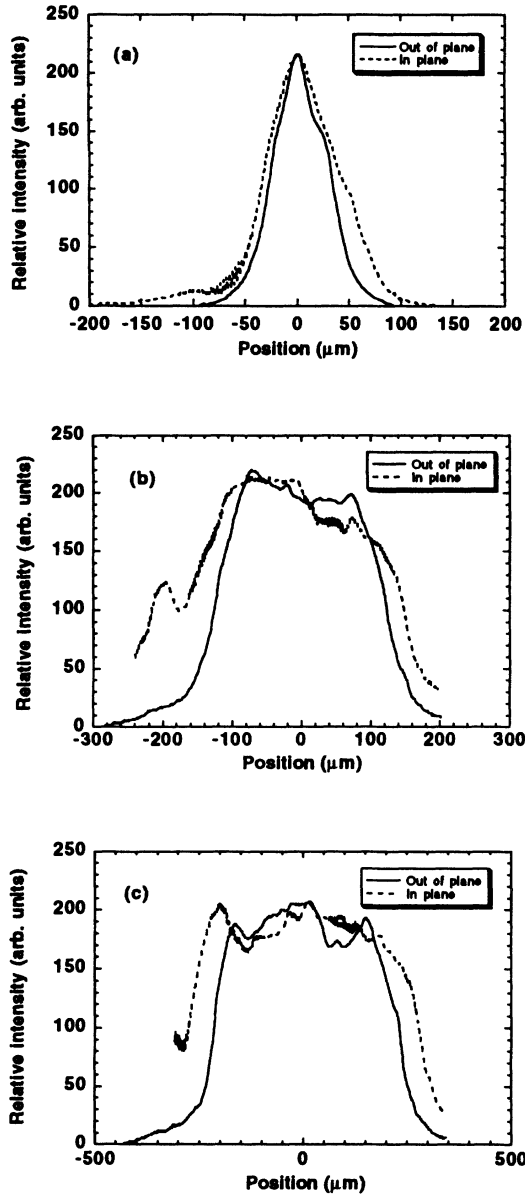


FIG. 1. The laser focal spot is measured by an equivalent plane imaging system. Vertical and horizontal intensity profiles of the laser spot have been taken for the cases where the spot diameter is (a) $100\ \mu\text{m}$, (b) $200\ \mu\text{m}$, and (c) $500\ \mu\text{m}$. The laser polarization was vertical for the data discussed in the text.

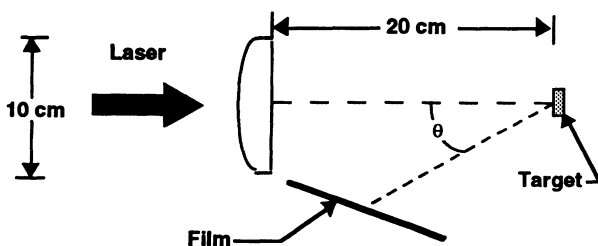


FIG. 2. The orientation of the recording film relative to the target and the incident laser beam and the target.

the film. The images were photodensitometered for analysis. Comparison of test exposures of $1\ \text{ns}$, $1.06\ \mu\text{m}$ laser pulses with different, but known, attenuation allowed us to calculate the relative intensity of the exposure from the film density [12].

We first discuss the angular variation of the scattered light intensity and then discuss the detailed structure. Figure 3 shows the results from a single laser pulse of $26\ \text{J}$ and $500\ \mu\text{m}$ spot diameter ($I_L = 1.3 \times 10^{13}\ \text{W}/\text{cm}^2$) in which separate pieces of film were located in and out of the plane of polarization. We clearly see a greater angular extent of the scattered light in the direction out of plane than in plane. Rotation of the polarization of the incident laser by a half-wave plate caused the pattern to also rotate, i.e., regardless of the orientation of the polarization, the scattered light in the out-of-plane direction was always of greater extent than in the plane of polarization. This result is in agreement with linear theory [4], which predicts a $\cos^2\phi$ dependence, where ϕ is the polar angle around the laser axis and $\phi=0^\circ$ corresponds to the plane containing the laser electric field, since the transverse electric fields of the incident and scattered light waves most effectively couple with the electric field of the electrostatic ion wave when $\phi=0^\circ$. Since the propagation vector of the scattered light wave was perpendicular to its electric field, this results in a peak in scattered light intensity in the direction $\phi=90^\circ$. Our observations show a different result than that found in Ref. [11], which observed no strong asymmetry relative to the polarization vector. The difference in that experiment is probably explained by the difference in the incident laser intensity used in each experiment; the intensity used in the experiments reported here are one to two orders of magnitude smaller than those reported in Ref. [11] (10^{15} – $10^{16}\ \text{W}/\text{cm}^2$). At such high intensities, the SBS instability, along with other parametric instabilities [13], is probably driven nonlinear and laser light can be scattered in the plane of polarization by high level density fluctuations.

Our observations show that the scattered light is dominated by stimulated Brillouin sidescattered light rather than by specularly scattered light. We collected the light scattered at 135° with respect to the incident laser and resolved it spectrally and temporally using a spectrome-

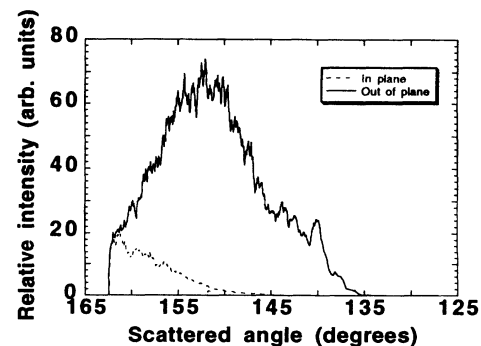


FIG. 3. Measured scattered light distribution in the plane of polarization and out of the plane of polarization. The laser pulse in this case was $26\ \text{J}$ and a $500\ \mu\text{m}$ spot diameter.

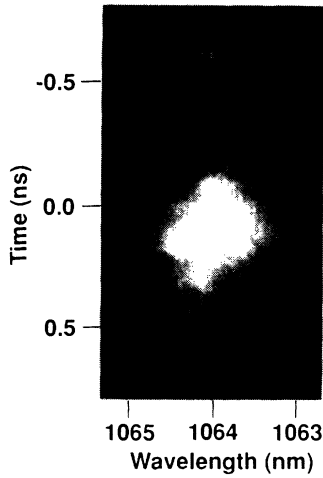


FIG. 4. Streak record of scattered light in the direction 45° with respect to the incident laser axis and out of the plane of polarization.

ter (1.4 Å resolution) and streak camera (20 ps resolution), respectively. A sample streak is shown in Fig. 4 for a laser pulse of 50 J and 500 μm spot diameter. The scattered signal has a different behavior than specular scatter in both wavelength and time. The time dependence of the scattered signal is quite different from that of the incident signal [see Fig. 5(a)]; after an initial burst, the scattered signal is low until the peak of the laser pulse when

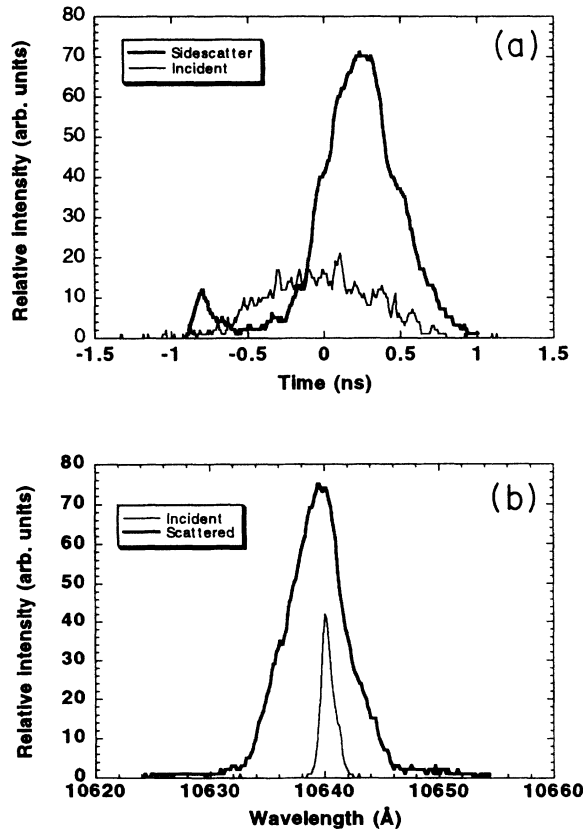


FIG. 5. Comparison between the incident laser pulse and the scattered signal in (a) time and (b) wavelength.

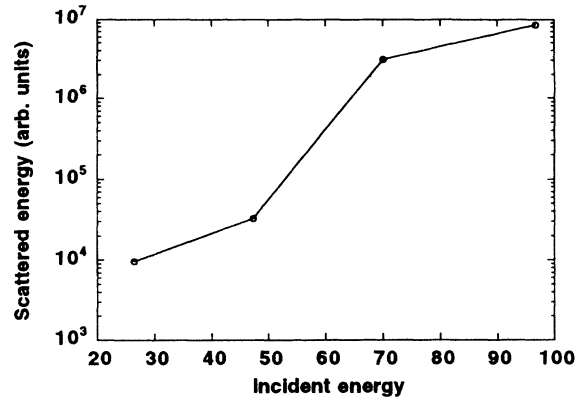


FIG. 6. Measured scattered light signal in the direction 45° with respect to the incident laser axis and out of the plane of polarization as a function of the incident laser energy. The laser spot diameter is 500 μm.

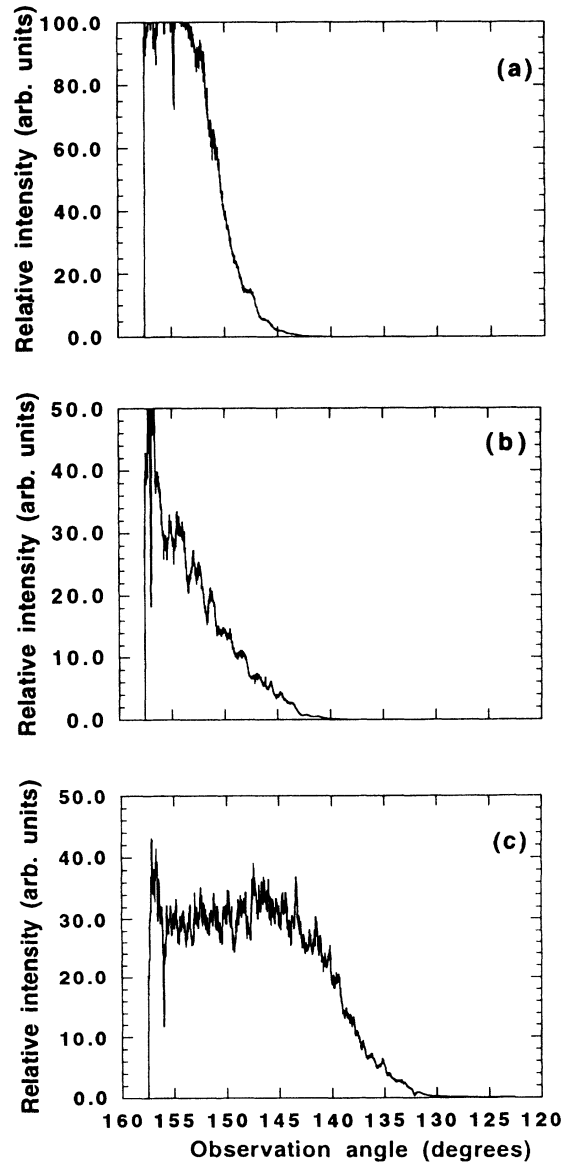


FIG. 7. Plot of scattered light intensity as a function of angle out of the plane of polarization for three different laser spot diameters: (a) 100 μm, (b) 200 μm, and (c) 500 μm.

the scattered signal abruptly turns on. The scattered signal is initially blueshifted [see Fig. 5(b)] and is significantly broader in wavelength than the incident laser (5 Å versus 1.4 Å bandwidth). It is difficult to explain how light reflected from the critical surface (the surface at which the laser frequency equals the plasma frequency) can blueshift the laser light since the critical surface is accelerated away by ablation from the laser (as confirmed by simulations). There is no obvious mechanism by which the critical surface can increase the bandwidth of the reflected light. SBS, on the other hand, is a known mechanism which can produce both a blueshift and bandwidth on the scattered light [17,18]. In addition, the total scattered signal (obtained by integrating the streak camera signal), grows exponentially with the incident laser intensity (see Fig. 6), another signature of

parametrically scattered light; the signal from light reflected from the critical surface should grow linearly.

The overall θ dependence of the scattered light depends on the laser spot size on the target. The scattered light covers a broader range of angles as the spot size is increased. This point is illustrated in Fig. 7 in which we show data from three separate target irradiations of different spot diameters (100, 200, and 500 μm) but similar intensity (2.7×10^{14} , 5.5×10^{13} , and 2.2×10^{13} W/cm^2 , respectively). The data have been averaged over $\pm 1^\circ$ in the ϕ direction.

The detailed structure of the scattered laser light also undergoes a change as the laser spot size is changed. As shown in Fig. 8, the scattered light pattern is not uniform, but has a structure which is smaller for larger spot diameters. We will discuss the observed structure and its relationship to the size of the scattering region in Sec. III C.

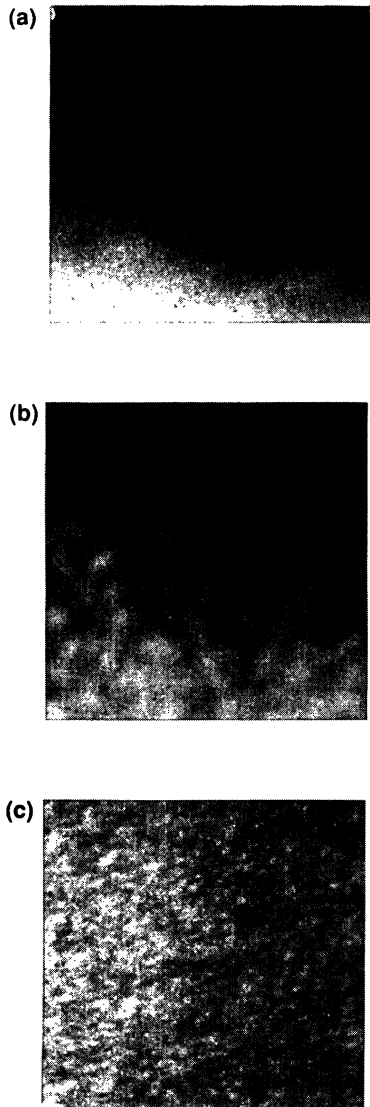


FIG. 8. Sample regions of the scattered light distribution for three different laser spot diameters: (a) 100 μm , (b) 200 μm , and (c) 500 μm . Each region was chosen from the center of each film and has dimensions of 2.5×2.5 cm^2 .

III. PREDICTIONS OF THE ANGULAR DEPENDENCE OF SBS

A. Analytic results

In this section we will derive the angular dependence of the SBS gain. Using this formula, we will calculate the convective growth of SBS as a function of scattering angle for a plasma profile predicted by LASNEX [14] for the parameters of our experiment. We then calculate the flux of the light scattered from the amplified ion acoustic waves as a function of angle. We take into account the refraction of the scattered light waves to produce a theoretical angular scattered light distribution that can be compared to our experiment.

We will consider convective growth of SBS for scattering angles between 90° and 180° . Absolute growth of SBS has been considered but is not applicable here [9]. Growth of SBS due to nonlocal thermal transport [15] has been discussed recently, but it predicts growth similar to ponderomotive theory for low Z targets as are used in our experiment.

The dispersion relation of the ion acoustic wave is given by (for $k_{ia}\lambda_D \ll 1$)

$$\omega_{ia} = k_{ia}c_s + \mathbf{k}_{ia} \cdot \mathbf{u} , \quad (1)$$

where ω_{ia} (k_{ia}) is the frequency (wave number) of the ion acoustic wave, $c_s = \sqrt{T_e/M_i}$ is the sound speed, and u is the expansion velocity (in this paper we will consider only the case where u is antiparallel to \mathbf{k}_0). For SBS to grow effectively, the following wave number and frequency matching conditions need to be satisfied:

$$\mathbf{k}_0 = \mathbf{k}_{ia} + \mathbf{k}_s , \quad (2a)$$

$$\omega_0 = \omega_{ia} + \omega_s , \quad (2b)$$

where the subscript s refers to the scattered electromagnetic wave. For the plasmas we have studied, $\omega_{ia} \approx 0.001\omega_0$, so $\omega \sim \omega_s$ and

$$k_{ia} \approx 2k_0 \sin(\theta/2) , \quad (3)$$

where θ is the angle of the scattered electromagnetic

wave with respect to \mathbf{k}_0 ($\theta = 180^\circ$ is direct backscatter).

We will consider convective growth of SBS for the case of \mathbf{k}_0 parallel to both ∇n and ∇u , but with arbitrary scattering angle. According to convective theory [3,8,16], the instability grows by e^G where the convective gain G is given by

$$G = 2\pi\gamma_0^2 / |\kappa'_z v_{ia,z} v_{s,z}|, \quad (4)$$

where γ_0 is the homogeneous growth rate given by (assuming a weak coupling between the pump wave and the ion wave) [2]

$$\gamma_0 = \omega_{pi} \frac{v_0}{2c} \left[\frac{ck_0}{\omega_0} \frac{c}{c_s} \frac{\sin(\theta/2)}{2} \right]^{1/2} \quad (5)$$

and ω_0 (k_0) is the incident laser frequency (wave number), ω_{pi} is the ion plasma frequency, and v_0 is the electron quiver velocity. The wave vector mismatch κ' in Eq.

$$|\kappa'_z v_{1z} v_{2z}| = [1 - M \sin(\theta/2)] \left\{ \frac{\omega_0}{2} \frac{c_s}{L_N} \frac{n_e}{n_c} (\cos\theta - 1) - k_{ia} c_s \left[\frac{-(1/2L_T) + [\sin(\theta/2)/L_u]}{\sin(\theta/2) - M} \right] \cos\theta (1 - n_e/n_c)^{1/2} \right\} \quad (8)$$

and

$$G \simeq \frac{(\pi/4)(v_0/v_e)^2 (n/n_c) k_0 L_u}{|D|}, \quad (9a)$$

where

$$D = (L_u/2L_N)(n_e/n_c)(\cos\theta - 1)[1 - M \sin(\theta/2)] - 2(1 - n_e/n_c) \sin(\theta/2) \cos\theta [\sin(\theta/2) - L_u/2L_T] \times [1 - M \sin(\theta/2)] / [\sin(\theta/2) - M]. \quad (9b)$$

The gradient scale lengths L_u , L_T , and L_N are defined as $L_u = c_s (du/dx)^{-1}$, $L_T = T_e (dT_e/dx)^{-1}$, and $L_N = n_e (dn_e/dx)^{-1}$. We find that for direct backscatter ($\theta = 180^\circ$), the gain formula reduces to that presented in Refs. [17] and [18].

Equation (9) predicts a very large sidescatter gain for scattering angles in the plasma near $\theta = 90^\circ$. This result is a consequence of the group velocity of the scattered light wave approaching zero at $\theta = 90^\circ$ [see Eq. (7a)]; the physical interpretation of this result is that, for a system of infinite transverse width, near $\theta = 90^\circ$, the scattered light wave propagates distances which are very long compared to the axial mismatch length before the wave refracts out of the phase-matching region. This problem has been avoided in previous discussions by restricting the use of Eq. (9) to certain regions of the plasma, e.g., $M \gg 1$ [8] or $n/n_c \ll 1$ [9]. We want to calculate the scattered light distribution from the entire plasma profile; for the purposes of this section we will use the fact that there is an implicit limit to the amount of growth of ion acoustic

(4) is given by

$$\kappa'_z = dk_{0,z}/dz - dk_{ia,z}/dz - dk_{s,z}/dz, \quad (6)$$

where z denotes the direction parallel to the target normal and the subscript z denotes the component of the wave numbers in the z direction. The group velocities of the ion acoustic wave and the scattered light wave are represented by v_{ia} and v_s , respectively. Their z components are given by

$$v_{s,z} = \frac{c}{\omega_s} (\omega_s^2 - \omega_{pe}^2)^{1/2} \cos\theta \quad (7a)$$

and

$$v_{ia,z} = [c_s - u \sin(\theta/2)] \sin(\theta/2), \quad (7b)$$

where u is the expansion velocity.

We find that

wave from thermal fluctuations to saturated levels, since fluctuations of $\delta n/n > 1$ are physically unrealistic. One estimate of this range is given by Ref. [19] as 10^5 . We have chosen to restrict e^G to less than 10^6 ; the overall angular distribution is not sensitive to the gain limit, although the value of the peak gain is very sensitive. In practice, the finite width of the plasma, the consequences of which we will discuss in Sec. IV, will restrict the sidescatter gain below the limit we set here.

Refraction of the scattered laser light significantly changes the angular distribution of the observed scattered light compared to that of the scattered light wave in the plasma. We formulate the refraction of the scattered light wave by allowing the wave vector to change in magnitude as it propagates into the vacuum due to the change in the plasma density while requiring the y component of the k vector to remain constant by conservation of y momentum. One can derive the following transformation, which is equivalent to Snell's law:

$$\sin\theta_{\text{obs}} = (1 - n_e/n_c)^{1/2} \sin\theta, \quad (10)$$

where θ is the scattering angle in the plasma and θ_{obs} is the observation angle in the vacuum. We then use the following equation [Eq. (25) of Ref. [20]] to calculate the scattered flux per unit solid angle per unit wavelength of light from a given gain:

$$F_L = \frac{ck_B T_L}{\lambda^4} E'' \frac{\omega_s}{2\omega_{ia}} \frac{\cos^2\theta_{\text{obs}}}{(\cos^2\theta_{\text{obs}} - \omega_p^2/\omega_s^2)^{1/2}} (e^G - 1), \quad (11)$$

where k_B is the Boltzmann constant and $E'' \approx 1$ is the transmission coefficient for light propagating from the interaction region to the vacuum.

We evaluate the angular distribution of SBS light using hydrodynamic profiles predicted by LASNEX simulations. The electron density, sound speed, and expansion velocity profiles at the peak of the laser pulse are shown in Fig. 9. We consider the profiles only at the peak of the laser pulse since we observe the maximum sidescatter signal near the peak of the laser pulse [see Fig. 5(a)]. The plasma parameters in each zone of the hydrodynamic simulation are used to evaluate Eqs. (9)–(11) to give the scattered light contribution for each observation angle. The amount of scattered light from each zone is subtracted from the incident laser intensity before calculating the next zone which is closer to the target.

The calculated angular distribution, which is the sum of the contributions from each underdense zone, is shown in Fig. 10. The scattered light peaks very strongly around an observed scattering angle of 130° . The scattered light at the peak of the angular distribution originates primarily from a zone with $n_e = 0.4n_c$. The calculation shows a much stronger peak and a broader angular spread which, while it agrees with the simulation results discussed below, is quite different from the observations of our experiment. In Sec. IV, we show that the assumption of a one-dimensional (1D) plasma that underlies our calculations is invalid and localization of the scattering region is required to match the experimental results.

B. Simulation results

We have also used simulations to study Brillouin scattering. The simulations serve as a check on the analytic theory presented in the preceding subsection and allow for the visualization of the ion density fluctuations involved in the instability. Here we briefly describe some

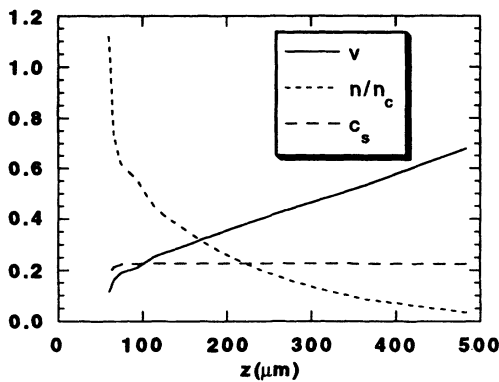


FIG. 9. Calculated one-dimensional LASNEX profiles for a solid CH target with $1.06 \mu\text{m}$ light at $I_L = 1 \times 10^{14} \text{ W/cm}^2$. The time frame is at the peak of a 1 ns Gaussian pulse. Shown are the relative density profile (n/n_c), the sound velocity profile (in units of 10^8 cm/s), and the expansion velocity profile (in units of 10^8 cm/s).

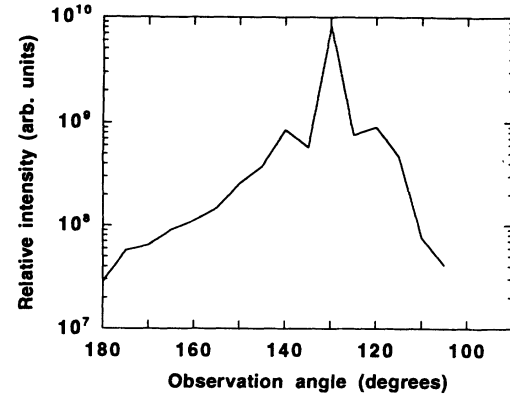


FIG. 10. Scattered light intensity versus angle calculated from the analytic formulation for sidescatter.

simulations using a two-dimensional one-fluid plasma model [21] that follows the behavior in the plane orthogonal to the direction of polarization of the light. Although this model does not include kinetic effects for the ions, it enables us to obtain some estimates of the angular behavior of sidescattering in larger systems than those which can be conveniently handled in a particle code. These simulations indicate that Brillouin sidescattering gives rise to angular lobes in the intensity of the reflected light. These lobes are preferentially out of the plane of polarization.

A simple example will be discussed. In this example, the plasma consists of a linear density ramp, rising from $n = 0.3n_c$ to $1.2n_c$ in a distance of $12.8\lambda_0$. The system is periodic in the other direction, which is the direction of the magnetic field of the incident light. The incident light intensity is $2.7 \times 10^{14} \text{ W/cm}^2$, the electron temperature is 0.5 keV, the viscous damping is small, and the mass ratio is 100. Absorption at the critical surface is crudely modeled by means of a collision frequency with a Lorentzian shape peaked at the critical density.

Figure 11 shows a surface plot of ion density at time $\omega_0 t = 3770$. Note the two-dimensional lattice of ion fluctuations that has been driven up by the back- and side-scattering in the underdense plasma. In this example, about 14% of the incident light is absorbed at the critical density (no inverse bremsstrahlung is included). The angular distribution of the scattered light, which includes light that is reflected at the critical surface, is shown in Fig. 12. Of particular interest are the angular lobes in the reflected light as a result of Brillouin sidescatter. Note that sidescattered light comes out of the plasma in this example with angles of about 143° to 157° , consistent with 90° sidescatter taking place at n_e about 0.6 – $0.9n_c$. Since this scattering preferentially occurs out of the plane of polarization, these angular lobes will be dominant in that direction.

This result is consistent with the results of analytic theory (see Fig. 10). The small difference in the scattering angle (10° – 20°) of the lobes predicted by the two methods is probably because the density profile used in the simulation was steeper than was used in Sec. III A.

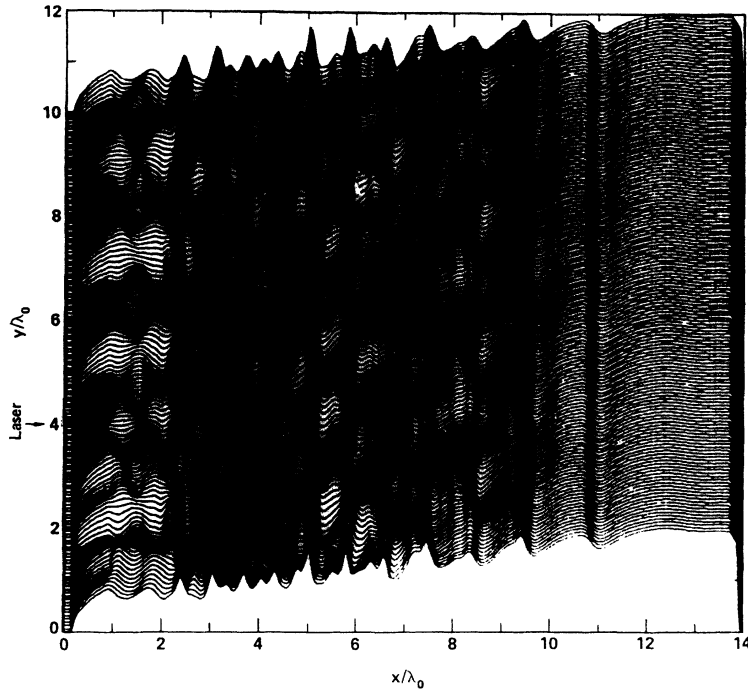


FIG. 11. Ion density surface after irradiation by plane *s*-polarized light incident from the left. The initial plasma density profile consisted of a linear ramp 0.3–1.2 times the critical density in 12.8 vacuum wavelengths and was 10 wavelengths wide. The height of the line is proportional to the relative density at that position. The electron temperature is 0.5 keV, the laser intensity is 2.7×10^{14} W/cm², and the snapshot is taken at time 600 laser cycles.

C. Small scale structure

The presence of a laser speckle pattern in the scattered light distribution from laser-produced plasmas has been previously discussed and presented for light backscattered into the focusing lens [22]. The speckle size provides a valuable indication of the size of the scattering region.

The size of the speckles at the film plane σ is given approximately by [23]

$$\sigma \approx 1.2\lambda z/D, \quad (12)$$

where λ ($=1.06 \mu\text{m}$) is the laser wavelength, z ($=10 \text{ cm}$) is the distance between the scattering point and the

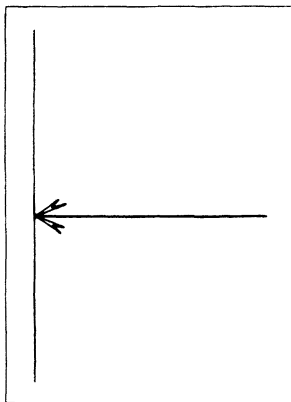


FIG. 12. Polar plot of the intensity of the reflected light versus angle, averaged from 500 to 600 laser cycles. The rippled ion density shown in Fig. 7 backscattered and sidescattered the light into this pattern.

recording film, and D is the diameter of the scattering region. Equation (12) predicts that the speckle size should decrease as the scattering region increases, which is observed in Fig. 8.

If we compare the size of the source region given by Eq. (12) to the laser spot diameter at the target, we find that the scattering region is the smaller of the two. Table I lists the source size calculated from Eq. (12) using the measured speckle size from the film data. It can be seen that the scattering region is at least a factor of 2 smaller than the laser diameter.

IV. DISCUSSION

The angular distribution of the scattered light observed in the experiment differs from that predicted in the preceding section. The difference is explained by the two-dimensional plasma distribution produced in the experiment which limits the SBS growth due to finite gradient scale lengths and finite extent of both the plasma and the pump laser.

As the spot diameter increases, the hydrodynamic expansion of the ablated plasma from a planar target changes from a two-dimensional expansion to a one-dimensional expansion. The transition occurs when the

TABLE I. Dependence of scattering size D on the focal spot diameter as calculated from Eq. (12) using the measured speckle size.

Spot diameter (μm)	σ (μm)	D (μm)
100	5.3	24
200	2.7	47
500	0.8	159

laser spot diameter is approximately equal to $c_s \tau_L$, where τ_L is the laser pulse length [24]. For the conditions of the experiment described in this paper, $c_s \approx 3 \times 10^7$ and $\tau_L = 1$ nsec, so two-dimensional expansion is expected for spot diameters less than $300 \mu\text{m}$. Small spots also reduce gradient scale lengths which result in reduced SBS growth.

The effect of the two dimensionality of the gain region is to limit SBS sidescattering growth. For direct sidescatter, the analytic theory predicts large gain because the interaction waves remain in the matching region until the scattered electromagnetic wave refracts out of it. If the electromagnetic wave leaves the plasma due to its finite extent, then the gain will be less than that predicted in Sec. III. We estimate the upper bound for the intensity gain to be

$$G = 2K_I L(\theta_s), \quad (13)$$

where [25]

$$K_I = \left[\frac{\gamma_0^2}{v_s v_{ia}} - \frac{1}{4} \left[\frac{\Gamma_1}{v_s} - \frac{\Gamma_2}{v_{ia}} \right]^2 \right] - \frac{1}{2} \left[\frac{\Gamma_1}{v_s} + \frac{\Gamma_2}{v_{ia}} \right] \quad (14)$$

is the homogeneous gain including the damping on the ion acoustic wave (Γ_2) and the electromagnetic wave (Γ_1). We neglect the damping on the electromagnetic wave. The damping on the ion acoustic wave in a CH plasma has been calculated recently [26] using a multiple kinetic model which takes into account multiple ion acoustic modes because of the presence of two atomic species. For $T_e \sim 0.8$ keV and $T_i \sim 0.3$ keV, the model predicts moderate damping ($\Gamma_2 \sim 0.1 \omega_{ia}$).

The result of limiting the transverse gain size is shown in Fig. 13. We have chosen the homogeneous growth length $L(\theta_s)$ to be $L / \sin(\theta_s)$, where L is the gain length in the direction transverse to the laser axis. The detailed functional form of $L(\theta_s)$ does not appear to be important as long as its value for direct backscatter, the direction for which we expect the inhomogeneous gain formula to be valid, is larger than the inhomogeneous mismatch length. As the size L is decreased, the angular extent is also decreased. The size of the gain region is also smaller than the initial laser spot size and is in qualitative agreement with the size of the gain region inferred from the speckle size (see Table I). Note that if we allow the transverse growth length to be as large as the spot size [see Fig. 13(d) where $L = 500 \mu\text{m}$], there is a significant disagreement with the observation.

The calculations (see Fig. 13) imply that the ion wave loses coherence with the pump wave within $30\text{--}60 \mu\text{m}$, which results in limited volumes of sufficient coherence for the ion wave to give large sidescatter. There are many processes such as competition between ion modes, turbulence, profile modification, or competition with stimulated Raman scattering which could produce this loss of coherence. The scattering volume can also be reduced if the laser beam filaments or self-focuses [28–31]. It is unlikely that this is due to ponderomotive filamentation which will produce hot spots of dimension $\sim 30 \mu\text{m}$ where the growth rate is maximized. If hot spots this size were contributing to SBS, then the source size would remain constant regardless of the laser spot size and the

scattered light distribution should be independent of the spot size, provided the laser intensity remains above the filamentation threshold.

Whole beam self-focusing of the beam can occur due to thermal filamentation which favors growth of filament sizes comparable to the laser beam diameter. The threshold intensity for thermal filamentation is [27]

$$I_t \approx 2 \times 10^{19} (n_c / n_e)^3 \frac{T_{\text{keV}}^5 \lambda_{\mu}^2}{Z^* L_{\mu}^2} \text{ W/cm}^2, \quad (15)$$

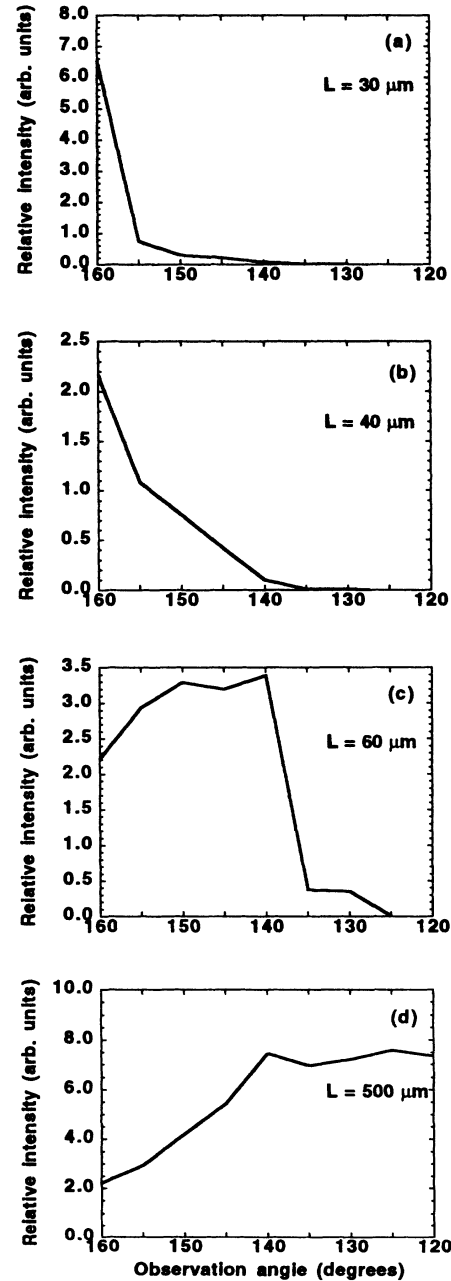


FIG. 13. Plots of calculated scattered light distribution using Eqs. (9)–(11) and assuming transverse gain lengths of (a) $L = 30 \mu\text{m}$, (b) $L = 40 \mu\text{m}$, (c) $L = 60 \mu\text{m}$, and (d) $L = 500 \mu\text{m}$. The angular distributions of (a)–(c) have angular distributions which are similar to the experimental results of Fig. 7.

where T_{keV} is the electron temperature in keV, λ_{μ} is the laser wavelength in micrometers, $Z^* = \langle Z^2 \rangle / \langle Z \rangle$ where Z is the charge state, and L_{μ} is the density gradient scale length in micrometers. Choosing $n_e \approx 0.5n_c$, $T_{\text{keV}} \sim 0.8$, $Z^* = 5$, and $L_{\mu} = 300 \mu\text{m}$ to match the experiment parameters gives $I_t \approx 2.5 \times 10^{13} \text{ W/cm}^2$, which is about the experimental intensity range.

V. CONCLUSIONS

Detailed measurements of laser light scattered from laser-produced plasmas show structure and angular distribution that evolve as the laser spot size is changed. The angular distribution is limited by two-dimensional plasma gradients that reduce stimulated Brillouin side-scattering in small plasmas. Even the largest spot diame-

ter ($500 \mu\text{m}$) examined in this paper has some 2D effect and does not replicate the predictions of 1D models.

Scattered light also exhibits structure, which we attribute to laser speckle. Speckle is independent of detailed structure that light scatters from, but can give an important indication of the size of the scattering volume.

ACKNOWLEDGMENTS

We thank J. Swain, P. Solone, and W. Cowens for laser support during this experiment. We also acknowledge useful conversations with E. A. Williams. This work was performed under the auspices of the U.S. Department of Energy by the Lawrence Livermore National Laboratory under Contract No. W-7405-Eng-48.

-
- [1] M. V. Goldman and D. F. DuBois, *Ann. Phys. (N.Y.)* **38**, 117 (1966).
 - [2] J. F. Drake, P. K. Kaw, Y. C. Lee, G. Schmidt, C. S. Liu, and M. N. Rosenbluth, *Phys. Fluids* **17**, 778 (1974).
 - [3] M. N. Rosenbluth, *Phys. Rev. Lett.* **29**, 565 (1972).
 - [4] C. S. Liu, M. N. Rosenbluth, and R. B. White, *Phys. Rev. Lett.* **31**, 697 (1973); *Phys. Fluids* **17**, 1211 (1974).
 - [5] C. E. Max, in *Laser-Plasma Interaction*, edited by R. Balian and J. C. Adam (North-Holland, Amsterdam, 1982), p. 301.
 - [6] D. Pesme, G. Laval, and R. Pellat, *Phys. Rev. Lett.* **31**, 203 (1973).
 - [7] D. DuBois, D. W. Forslund, and E. A. Williams, *Phys. Rev. Lett.* **33**, 1013 (1973).
 - [8] C. S. Liu, in *Advances in Plasma Physics*, edited by A. Simon and W. B. Thomson (Interscience, New York, 1976), Vol. 6, pp. 47 and 145.
 - [9] R. L. Berger, *Phys. Fluids* **27**, 1796 (1984).
 - [10] R. A. Haas, W. C. Mead, W. L. Kruer, D. W. Phillion, H. N. Kornblum, J. D. Lindl, D. MacQuigg, V. C. Rupert, and K. G. Tirsell, *Phys. Fluids* **20**, 322 (1977); M. D. Rosen, D. W. Phillion, V. C. Rupert, W. C. Mead, W. L. Kruer, J. J. Thomson, H. N. Kornblum, V. W. Slivinski, G. J. Caporaso, M. J. Boyle, and K. G. Tirsell, *Phys. Fluids* **22**, 2020 (1979).
 - [11] B. H. Ripin, *Appl. Phys. Lett.* **30**, 134 (1977).
 - [12] See National Technical Information Service Document No. UCRL-50021-76. [G. G. Peterson, Lawrence Livermore National Laboratory, Laser Program Annual Report No. UCRL-50021-76, pp. 2-364, 1976 (unpublished).] Copies may be ordered from the National Technical Information Service, Springfield, VA 22161. The price is \$105.00 plus a \$3.00 handling fee. All orders must be prepaid.
 - [13] P. E. Young, B. F. Lasinski, W. L. Kruer, E. A. Williams, K. G. Estabrook, E. M. Campbell, R. P. Drake, and H. A. Baldis, *Phys. Rev. Lett.* **61**, 2766 (1988).
 - [14] G. D. Zimmerman and W. L. Kruer, *Comm. Plasma Phys. Controlled Fusion* **2**, 51 (1977).
 - [15] R. W. Short and E. M. Epperlein, *Phys. Rev. Lett.* **68**, 3307 (1992).
 - [16] C. S. Liu, M. N. Rosenbluth, and R. B. White, *Phys. Fluids* **17**, 1211 (1974).
 - [17] P. E. Young, K. G. Estabrook, W. L. Kruer, E. A. Williams, P. J. Wegner, R. P. Drake, H. A. Baldis, and T. W. Johnston, *Phys. Fluids B* **2**, 1907 (1990).
 - [18] P. E. Young, R. L. Berger, and K. G. Estabrook, *Phys. Fluids B* **4**, 2605 (1992).
 - [19] C. J. Randall, J. R. Albritton, and J. J. Thomson, *Phys. Fluids* **24**, 1474 (1981).
 - [20] R. L. Berger, E. A. Williams, and A. Simon, *Phys. Fluids B* **1**, 414 (1989).
 - [21] E. J. Valeo and K. Estabrook, *Phys. Rev. Lett.* **34**, 1008 (1975); K. Estabrook, *Phys. Fluids* **19**, 1733 (1976).
 - [22] R. A. M. Maddever, B. Luther-Davies, and R. Dragila, *Phys. Rev. A* **41**, 2154 (1990); **41**, 2165 (1990).
 - [23] A. E. Ennos, in *Laser Speckle and Related Phenomena*, edited by J. C. Dainty, *Topics in Applied Physics* Vol. 9 (Springer-Verlag, Berlin, 1975), pp. 203-253.
 - [24] P. Mora and R. Pellat, *Phys. Fluids* **22**, 2300 (1979).
 - [25] K. Nishikawa, in *Advances in Plasma Physics* (Ref. [8]), Vol. 6, p. 37.
 - [26] E. A. Williams and R. L. Berger, private communication.
 - [27] W. L. Kruer, *Comments Plasma Phys. Controlled Fusion* **9**, 63 (1985).
 - [28] P. E. Young, *Comments Plasma Phys. Controlled Fusion* **12**, 53 (1988).
 - [29] P. E. Young, H. A. Baldis, R. P. Drake, E. M. Campbell, and K. G. Estabrook, *Phys. Rev. Lett.* **61**, 2336 (1988).
 - [30] E. Epperlein, *Phys. Rev. Lett.* **65**, 2145 (1990).
 - [31] P. E. Young, *Phys. Fluids B* **3**, 2331 (1991).

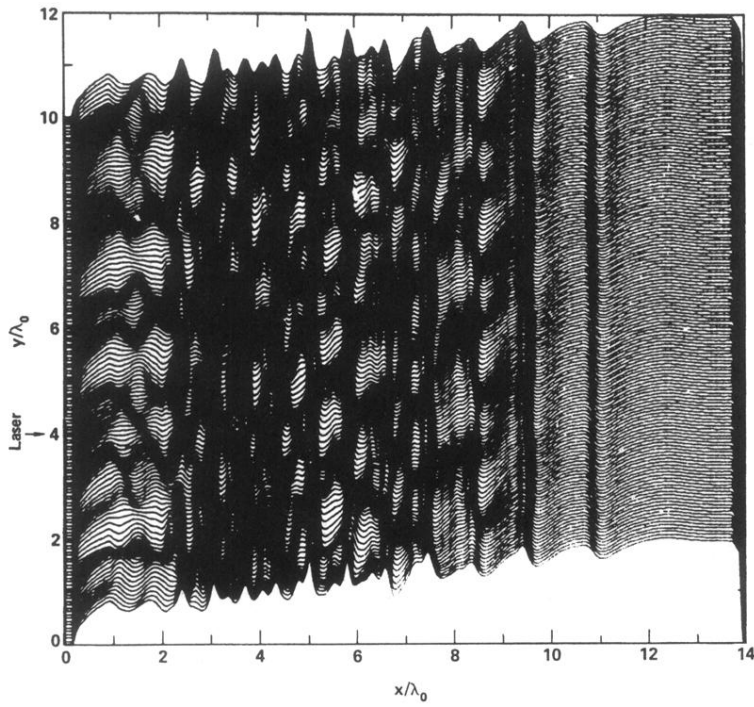


FIG. 11. Ion density surface after irradiation by plane *s*-polarized light incident from the left. The initial plasma density profile consisted of a linear ramp 0.3–1.2 times the critical density in 12.8 vacuum wavelengths and was 10 wavelengths wide. The height of the line is proportional to the relative density at that position. The electron temperature is 0.5 keV, the laser intensity is 2.7×10^{14} W/cm², and the snapshot is taken at time 600 laser cycles.

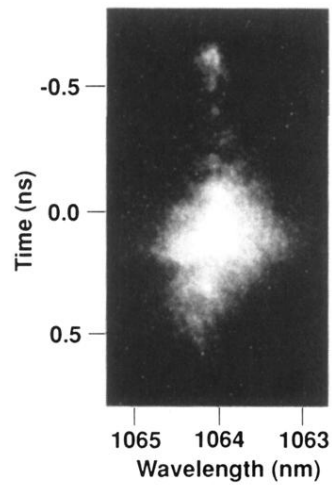


FIG. 4. Streak record of scattered light in the direction 45° with respect to the incident laser axis and out of the plane of polarization.

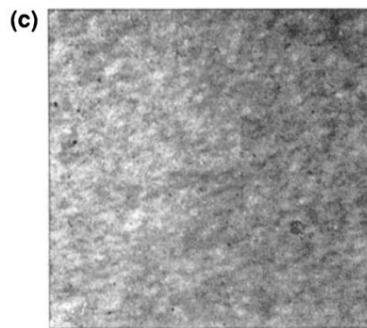
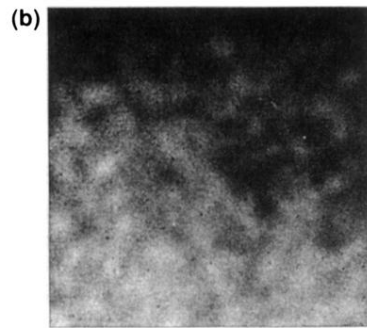
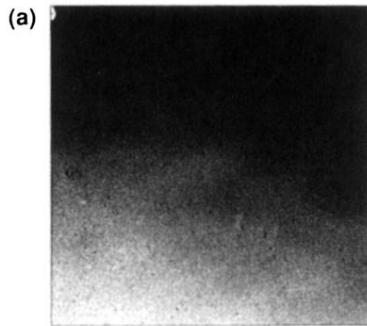


FIG. 8. Sample regions of the scattered light distribution for three different laser spot diameters: (a) $100\ \mu\text{m}$, (b) $200\ \mu\text{m}$, and (c) $500\ \mu\text{m}$. Each region was chosen from the center of each film and has dimensions of $2.5 \times 2.5\ \text{cm}^2$.